Supplemental Materials for

Source mechanism of a lower crust earthquake beneath the Himalayas and its possible relation to metamorphism

Celso Alvizuri and György Hetényi

July 19, 2019

List of Figures

Overview

This supplement contains figures related to the moment tensor analysis for our main Himalaya earthquake on 2002-05-08 and a smaller earthquake on 2001-10-24.

References

Alvizuri, C., V. Silwal, L. Krischer, and C. Tape (2018), Estimation of full moment tensors, including uncertainties, for nuclear explosions, volcanic events, and earthquakes, *J. Geophys. Res. Solid Earth*, *123*, 5099–5119, doi:10.1029/2017JB015325.

Monsalve, G., A. Sheehan, V. Schulte-Pelkum, S. Rajaure, M. R. Pandey, and F. Wu (2006), Seismicity and one-dimensional velocity structure of the Himalayan collision zone: Earthquakes in the crust and upper mantle, *J. Geophys. Res.*, *111*(B10301), doi:10.1029/2005JB004062.

Tape, W., and C. Tape (2012), A geometric setting for moment tensors, *Geophys. J. Int.*, *190*, 476–498, doi:10.1111/j.1365-246X.2012.05491.x.

Tape, W., and C. Tape (2013), The classical model for moment tensors, *Geophys. J. Int.*, *195*, 1701–1720, doi:10.1093/gji/ggt302.
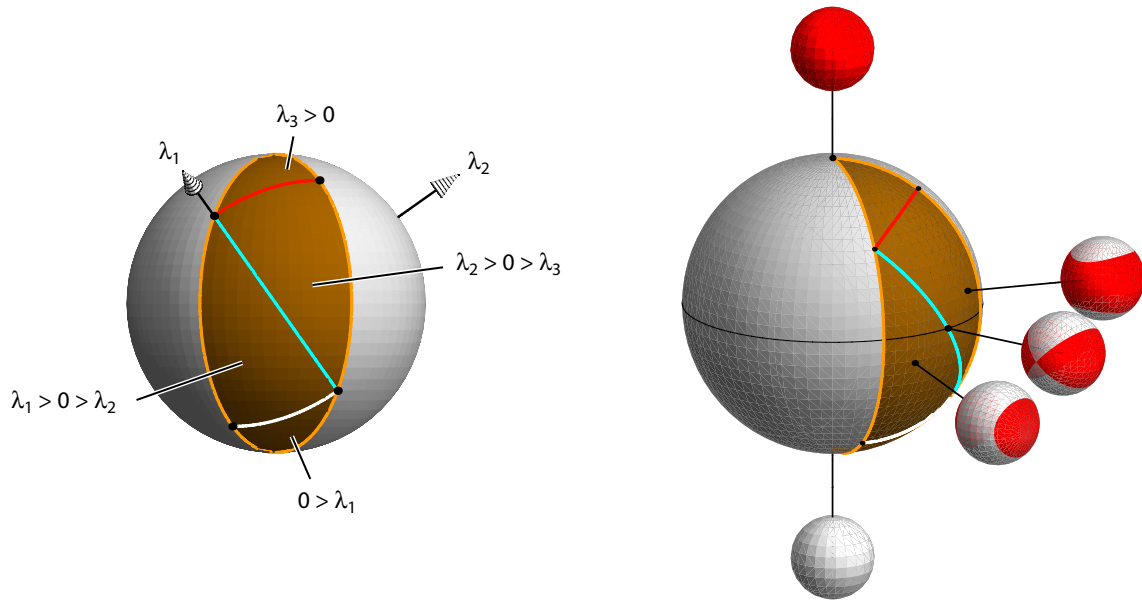
Figure S1: Four regimes for moment tensors on the fundamental lune (Figure S1 from *Tape and Tape*, 2013). The eigenvalues $(\lambda_1, \lambda_2, \lambda_3)$ of a seismic moment tensor can be organized on a section of a sphere, or lune, where $\lambda_1 \geq \lambda_2 \geq \lambda_3$ (*Tape and Tape*, 2012). The moment tensor eigenvalues determine the shading on the beachballs, and they also separate the lune into four main regimes. Moment tensor beachballs above the arc $\lambda_3 = 0$ are colored all red, and beachballs below the arc $\lambda_1 = 0$ are colored all white. The diagonal (cyan) arc $\lambda_2 = 0$ separates beachballs into those with red caps and white bands ($\lambda_1 > 0 > \lambda_2$), and those with white caps and red bands ($\lambda_2 > 0 > \lambda_3$). The double-couple is at the center of the lune.
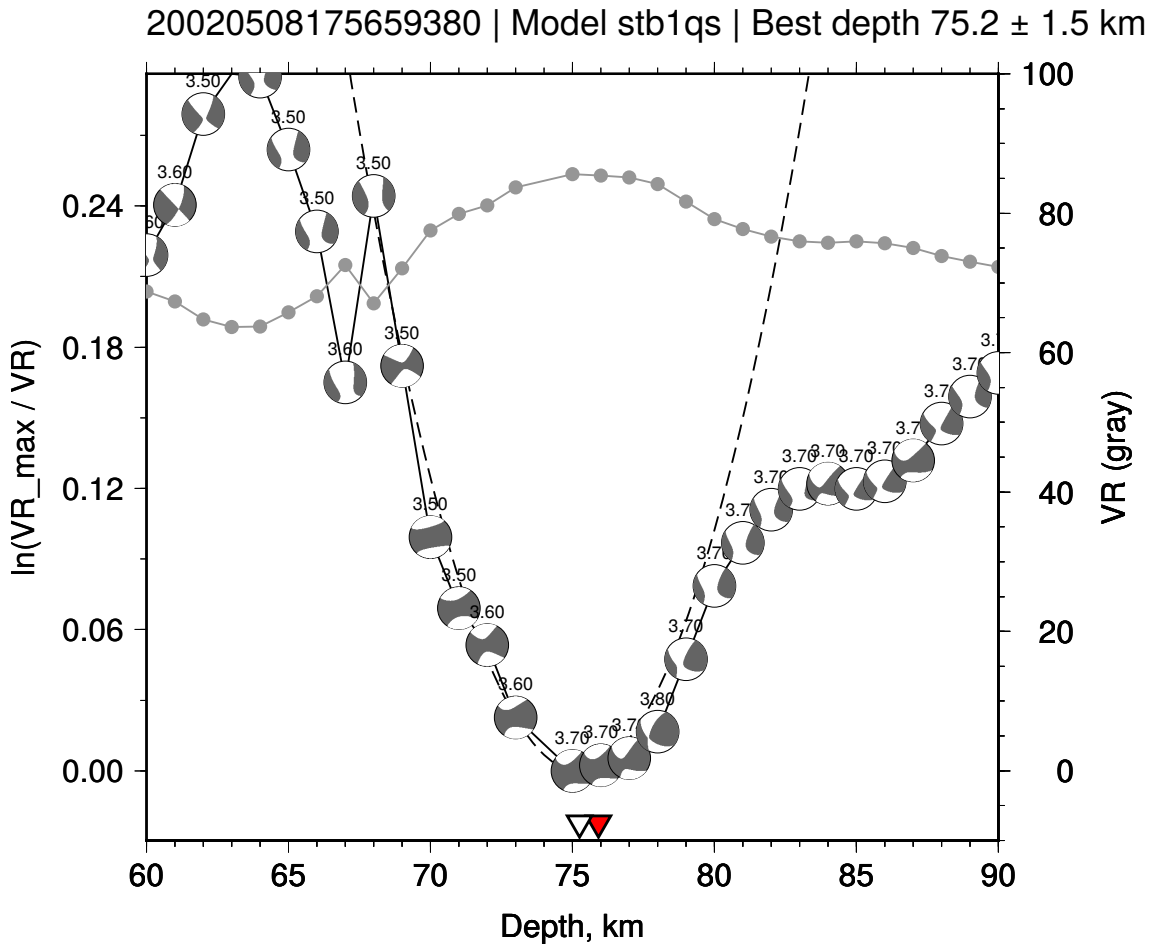
Figure S2: Grid search over depth for the best moment tensor for the Himalaya earthquake analyzed here. Each beachball shows the best-fitting moment tensor (and magnitude) for a particular depth. The right axis shows the variance reduction (light gray curve). The left axis shows the deviation in variance reduction from the global minimum (black curve) at 75 km. The white triangle is the global minimum, the red triangle is the catalog depth from *Monsalve et al.* (2006). The plot reveals an optimal depth between 73 and 77 km.

Caption for figure S3 (next page). Full moment tensor uncertainty summary for the Himalaya main event, Figure **??**. This representation follows *Alvizuri et al.* (2018). (a) Map of source location (red star) and stations used in the inversion for this event. The station is colored blue if the observed first-motion polarity on the vertical component is up (compression) and white if it is down (dilatation). (b) Contour plot of the polarity misfit on the lune. (c) Source type probability density $p(v, w)$ in the vw rectangle. A green square indicates the location of the point (v_x, w_x) where p is maximum; this point is apt to differ from the source type (v_0, w_0) of M_0. (d) Contour plot of the variance reduction $VR(\mathbf{\Lambda})$. At each point $\mathbf{\Lambda}$, the variance reduction $VR(\mathbf{\Lambda})$ is the maximum variance reduction $VR(M)$ for moment tensors M that have source type $\mathbf{\Lambda}$. Large values (blue) of VR represent better fit between observed and synthetic waveforms. Of the beachballs $M(\mathbf{\Lambda})$, our solution M_0 (green circle) is the one with largest VR. The gray arcs on the lune are the great circle arcs $\lambda_1 = 0$, $\lambda_2 = 0$, and $\lambda_3 = 0$. Selected eigenvalue triples (black dots) on the boundary of the lune are indicated, with the understanding that the triples need to be normalized. The positive isotropic source $(1, 1, 1)$ is at the top, the negative isotropic source $(-1, -1, -1)$ is at the bottom, and the double couple $(1, 0, -1)$, not shown, would be at the center of the lune. (e) The curves $\hat{V}'(\omega)$ and $\hat{P}'(\omega)$ that are used to construct the confidence curve $\mathscr{P}(V)$ in (f). For full moment tensors, as here, $\hat{V}'(\omega) \propto \sin^4 \omega$. (f) The confidence curve $\mathscr{P}(V)$ for M_0. The more the curve resembles the shape of a capital gamma (Γ), the better. The shaded area is the average confidence $\mathscr{P}_{\mathrm{AV}}$. (g) The moment tensor M_0, plotted in a lower-hemisphere projection. The location of the piercing point for each station depends on the station azimuth, epicentral distance, and the assumed layered reference model.

Event 20020508175659380, M 3.70
Lon 86.4885, Lat 28.5825
Dep 75.9 km (inversion 76 km)
$(\gamma, \delta)_{VR}^{max} = (-5°, 17°)$ $(\gamma, \delta)_{p}^{max} = (22°, 26°)$

(a)

(b)

[No polarities]

(c)

(d)

(e)

(f)

(g)

Figure S3:

5

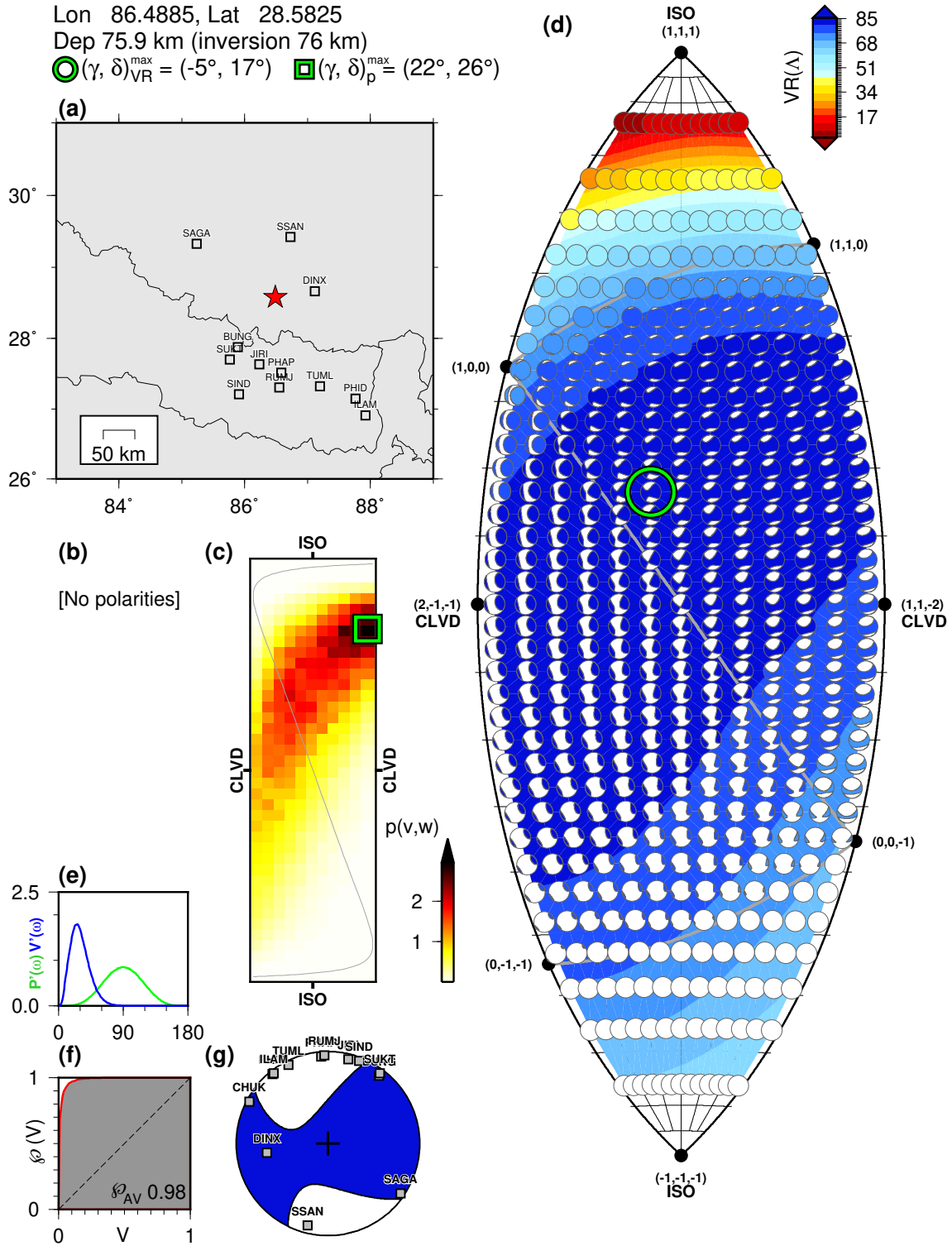Event 20020508175659380
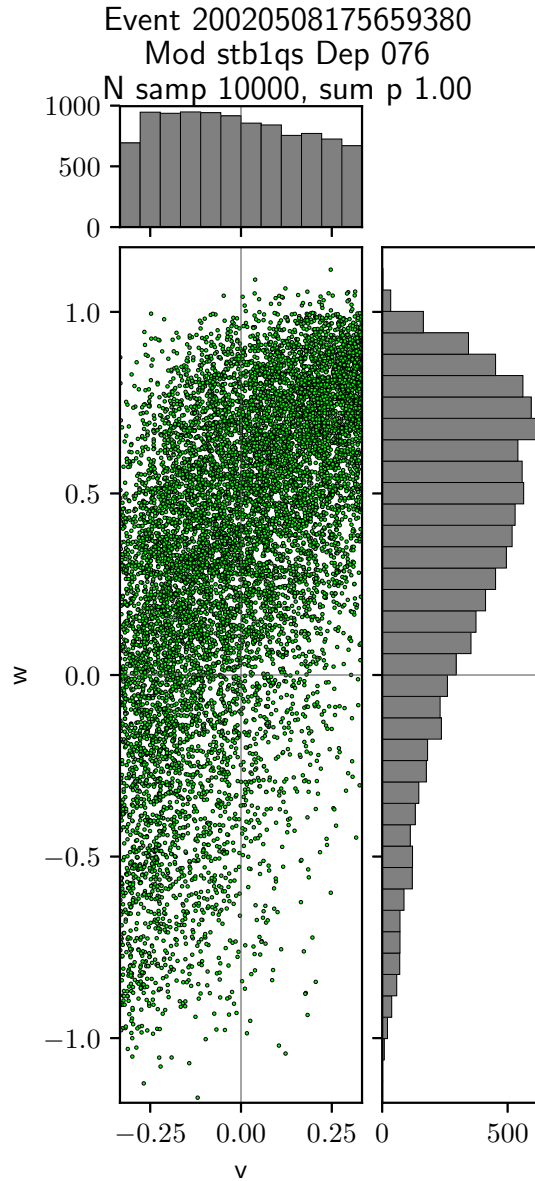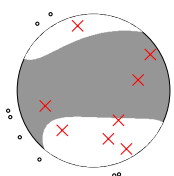Mod stb1qs Dep 076
N samp 10000, sum p 1.00

Figure S4: Posterior samples from the moment tensor uncertainty analysis for the Himalaya main event. The green circles are pairs (v, w) for a set of 10000 posterior samples from the probability density $p(v, w)$ shown in Figure **??**c and Figure S3c. We used these samples to derive the histograms in Figure **??**.

Event 200110240803100030 Model stb1qs Depth 68
FM 229 37 45 Mw 2.60 γ 9 δ 10 rms 6.742e−01 VR 54.5 pol_wt 999.00
Filter periods (seconds): Body:0.67−1.67. Surf:16.67−25.00 duration: 0.08/0.04 s
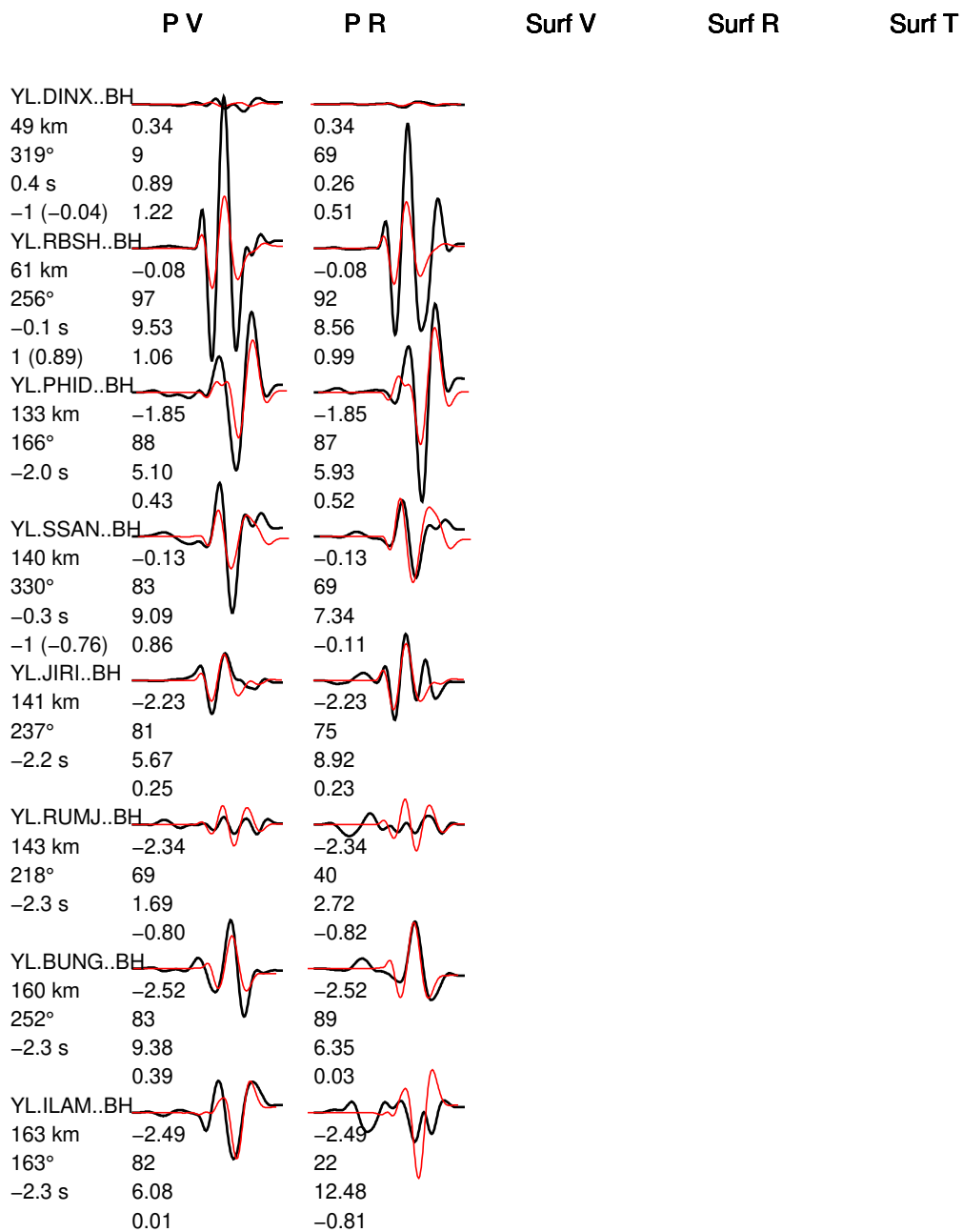# norm L1   # Pwin 5 Swin 300   # N 8 Np 16 Ns 0

P V   P R   Surf V   Surf R   Surf T

YL.DINX..BH
49 km   0.34   0.34
319°   9   69
0.4 s   0.89   0.26
−1 (−0.04)   1.22   0.51
YL.RBSH..BH
61 km   −0.08   −0.08
256°   97   92
−0.1 s   9.53   8.56
1 (0.89)   1.06   0.99
YL.PHID..BH
133 km   −1.85   −1.85
166°   88   87
−2.0 s   5.10   5.93
             0.43   0.52
YL.SSAN..BH
140 km   −0.13   −0.13
330°   83   69
−0.3 s   9.09   7.34
−1 (−0.76)   0.86   −0.11
YL.JIRI..BH
141 km   −2.23   −2.23
237°   81   75
−2.2 s   5.67   8.92
             0.25   0.23
YL.RUMJ..BH
143 km   −2.34   −2.34
218°   69   40
−2.3 s   1.69   2.72
             −0.80   −0.82
YL.BUNG..BH
160 km   −2.52   −2.52
252°   83   89
−2.3 s   9.38   6.35
             0.39   0.03
YL.ILAM..BH
163 km   −2.49   −2.49
163°   82   22
−2.3 s   6.08   12.48
             0.01   −0.81

Figure S5: Moment tensor solution and waveform fits for the second earthquake considered here, on 2001-10-24.
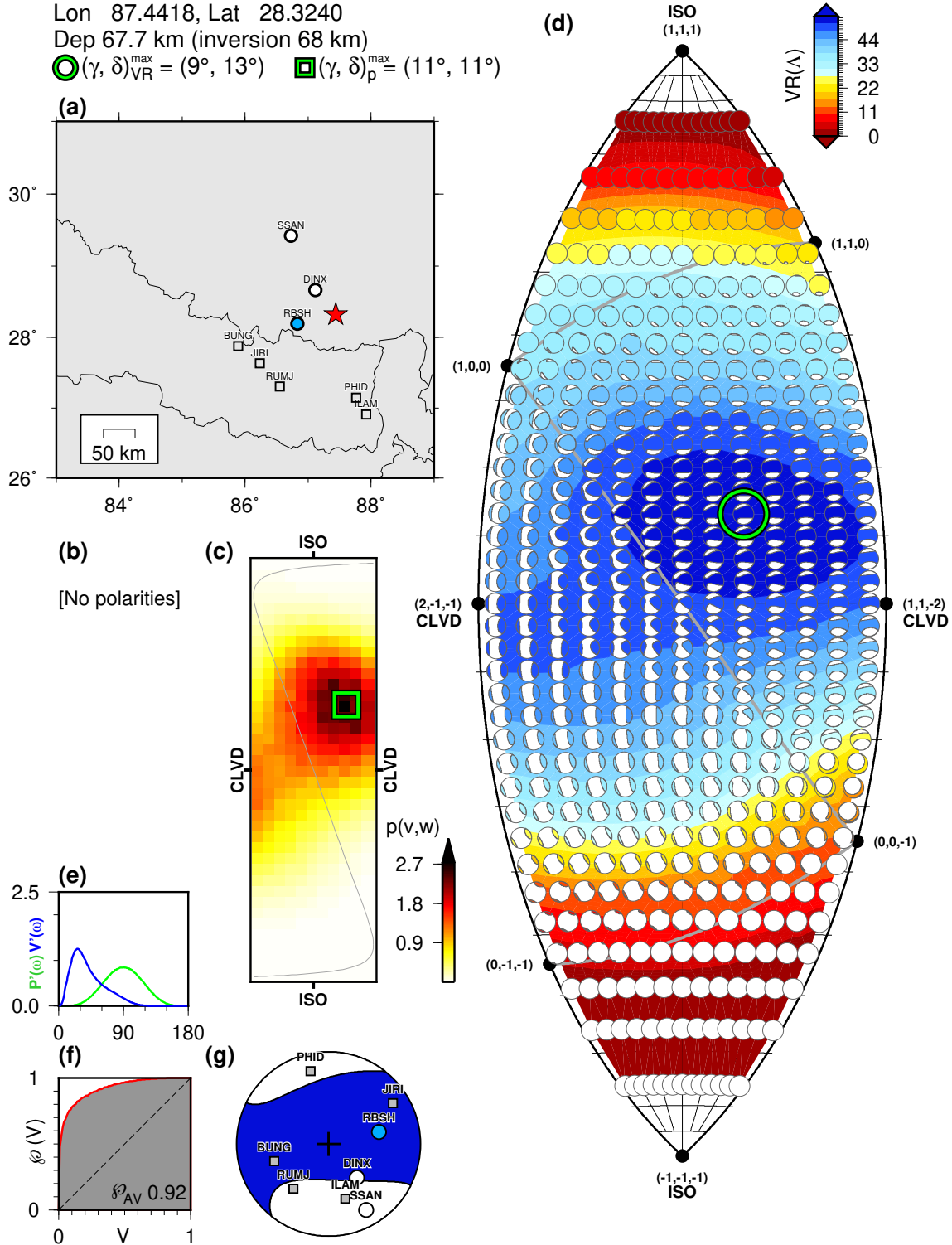
Figure S6: Full moment tensor uncertainty analysis for the result in Figure S5. See the caption in Figure S3 for details.